THE JOURNAL OF BIOLOGICAL CHEMISTRY VOL. 288, NO. 34, pp. 24705–24716, August 23, 2013

Energy Transducing Roles of Antiporter-like Subunits in *Escherichia coli* NDH-1 with Main Focus on Subunit NuoN (ND2)*

Received for publication, May 3, 2013, and in revised form, July 9, 2013 Published, JBC Papers in Press, July 17, 2013, DOI 10.1074/jbc.M113.482968

Motoaki Sato[1], **Prem Kumar Sinha, Jesus Torres-Bacete**[2], **Akemi Matsuno-Yagi, and Takao Yagi**[3]

From the ‡Department of Molecular and Experimental Medicine, MEM-256, The Scripps Research Institute, La Jolla, California 92037

Background: Antiporter-like subunits NuoL, NuoM, and NuoN are structurally similar but whether NuoN functions as a proton pump was uncertain.
Results: Functionally and structurally important residues in NuoN were identified.
Conclusion: NuoN is involved in proton translocation.
Significance: Similarities and differences of essential residues for proton translocation in the antiporter-like subunits were disclosed.

The proton-translocating NADH-quinone oxidoreductase (complex I/NDH-1) contains a peripheral and a membrane domain. Three antiporter-like subunits in the membrane domain, NuoL, NuoM, and NuoN (ND5, ND4 and ND2, respectively), are structurally similar. We analyzed the role of NuoN in *Escherichia coli* NDH-1. The lysine residue at position 395 in NuoN ($_{N}$Lys^{395}) is conserved in NuoL ($_{L}$Lys^{399}) but is replaced by glutamic acid ($_{M}$Glu^{407}) in NuoM. Our mutation study on $_{N}$Lys^{395} suggests that this residue participates in the proton translocation. Furthermore, we found that $_{M}$Glu^{407} is also essential and most likely interacts with conserved $_{L}$Arg^{175}. Glutamic acids, $_{N}$Glu^{133}, $_{M}$Glu^{144}, and $_{L}$Glu^{144}, are corresponding residues. Unlike mutants of $_{M}$Glu^{144} and $_{L}$Glu^{144}, mutation of $_{N}$Glu^{133} scarcely affected the energy-transducing activities. However, a double mutant of $_{N}$Glu^{133} and nearby $_{K}$Glu^{72} showed significant inhibition of these activities. This suggests that $_{N}$Glu^{133} bears a functional role similar to $_{L}$Glu^{144} and $_{M}$Glu^{144} but its mutation can be partially compensated by the nearby carboxyl residue. Conserved prolines located at loops of discontinuous transmembrane helices of NuoL, NuoM, and NuoN were shown to play a similar role in the energy-transducing activity. It seems likely that NuoL, NuoM, and NuoN pump protons by a similar mechanism. Our data also revealed that $_{N}$Lys^{158} is one of the key interaction points with helix HL in NuoL. A truncation study indicated that the C-terminal amphipathic segments of $_{N}$TM14 interacts with the $_{M}\beta$ sheet located on the opposite side of helix HL. Taken together, the mechanism of H^+ translocation in NDH-1 is discussed.

The proton-translocating NADH-quinone oxidoreductase (complex I)[4] (EC 1.6.5.3) is the first enzyme of the respiratory chain in most eukaryotic cells (1). Complex I catalyzes the electron transfer from NADH to quinone, which is coupled to the translocation of protons through the inner mitochondrial membrane (2). This enzyme complex, made up of ~45 different polypeptides, is the largest enzyme of the respiratory chain, with a molecular mass of ~1,000 kDa (1, 3). The physiological importance of complex I is highlighted by the fact that this enzyme is the principal source of reactive oxygen species in mitochondria and that its deficiencies are linked to many human diseases (4). The bacterial enzyme (NDH-1) is composed only of 13–14 subunits with a molecular mass of 500 kDa (5), all of which are homologous to the 14 subunits that constitute the core of the mitochondrial complex I (6). Both eukaryotic complex I and prokaryotic NDH-1 have a characteristic L-shaped form with two clearly defined domains, a hydrophilic peripheral domain and a hydrophobic domain (7). The hydrophilic domain is projected into the mitochondrial matrix/bacterial cytoplasm and houses all of the cofactors that participate in electron transfer from NADH to quinone, through FMN and a chain of seven conserved Fe/S clusters (8–15). In *Escherichia coli*, the hydrophilic domain contains six subunits named NuoB, NuoCD (a fusion of 2 subunits, NuoC and NuoD), NuoE, NuoF, NuoG, and NuoI.

The hydrophobic membrane domain is embedded in the inner mitochondrial/cytoplasmic membrane and is believed to participate in H^+ translocation and in the binding of quinone and specific inhibitors (6, 16). For functional study of the NDH-1/complex I, it is a prerequisite to clarify sites and mechanisms

* This work was supported, in whole or in part, by National Institutes of Health United States Public Health Service Grant GM33712 (to T. Y.).
[1] On leave from Odawara Research Center, Nippon Soda Co., Ltd., Odawara 250-0280, Japan.
[2] Present address: Centro de investigaciones Biologicas del CSIC, Madrid, 28040 Madrid, Spain.
[3] To whom correspondence should be addressed: 10550 N. Torrey Pines Rd., MEM256, La Jolla, CA 92037. Fax: 858-784-2054; E-mail: yagi@scripps.edu.

[4] The abbreviations used are: complex I, mitochondrial proton-translocating NADH-quinone oxidoreductase; NDH-1, bacterial proton-translocating NADH-quinone oxidoreductase; DB, 2,3-dimethoxy-5-methyl-6-decyl-1,4-benzoquinone; dNADH, reduced nicotinamide hypoxanthine dinucleotide; oxonol VI, bis-(3-propyl-5-oxoisoxazol-4-yl)pentamethine oxonol; ACMA, 9-amino-6-chloro-2-methoxyacridine; FCCP, carbonyl cyanide *p*-trifluoromethoxy phenylhydrazone; TM, transmembrane segment(s); BisTris, 2-[bis(2-hydroxyethyl)amino]-2-(hydroxymethyl)propane-1,3-diol; BN, blue native.

of the H^+ translocation. The membrane domain of *E. coli* NDH-1 is composed of seven subunits, NuoA, NuoH, NuoJ, NuoK, NuoL, NuoM, and NuoN, which are homologues of the mitochondrial DNA-encoded subunits, ND3, ND1, ND6, ND4L, ND5, ND4, and ND2, respectively.

According to the recently disclosed three-dimensional structures of the transmembrane segment of complex I/NDH-1 (7, 17–19), subunits NuoA, NuoJ, NuoK, and NuoH are located close to the peripheral arm, whereas subunits NuoL, NuoM, and NuoN are in the extended part of the membrane arm. The structural model revealed that NuoL, NuoM, and NuoN share similar structural features with multisubunit antiporters (20, 21) and energy-converting NiFe hydrogenases (22), leading to a hypothesis that they have evolved from a common ancestor (23). This suggests involvement of the antiporter-like subunits in the mechanism of H^+ translocation. Their distal location from the electron transfer pathway and their side-by-side arrangement strongly suggested a long range conformational change as an essential part of the energy-coupling mechanism of complex I/NDH-1 (6, 18, 24).

The three-dimensional structure also showed that the longest subunit, NuoL, possesses a long amphipathic α-helix (110 Å in case of *E. coli*), called helix HL, spanning and making a bridge among NuoK, NuoN, NuoM, and NuoL (7). On the opposite side of helix HL, there are long β sheets in NuoM and NuoL linking themselves to neighboring subunits NuoN and NuoM, respectively. Sazanov and co-workers (7, 17) have hypothesized that helix HL can work in a piston-like mechanism, together with the β sheets, driving the conformational changes along the antiporter-like subunits.

Our mutation studies of membrane domain subunits NuoA, NuoJ, NuoK, NuoH, NuoM, and NuoL showed that NuoK, NuoM, and NuoL are directly involved in the H^+ translocation (25–31). The stoichiometry of the H^+ translocation in NDH-1/complex I is long believed to be 4 $H^+/2e^-$ per NADH oxidized (32). Recently, an alternative stoichiometry of 3 $H^+/2e^-$ under certain conditions was reported (2). Yet another study reported that NDH-1/complex I lacking both NuoL and NuoM can pump two protons with a stoichiometry of $H^+/2e^- = 2$ (33, 34). These data suggest that NDH-1/complex I may contain either 3 or 4 H^+ translocation sites, also implying the possibility of the H^+ translocation in NuoN.

The NDH-1 crystal structure showed that NuoN is located close to the NuoAJK bundle (7, 17). Previously Amarneh and Vik (35) reported that conserved lysine residues in the middle of the transmembrane helices were required for the energy-transducing NDH-1 activity and that mutation of conserved $_N$Glu^{133} in the membrane helix only moderately (30%) reduced the energy-transducing NDH-1 activities. On the other hand, we and others showed that mutations of corresponding glutamic acids in NuoM and NuoL lead to almost total elimination of energy-transducing NDH-1 activities (24, 27, 36). These reports suggest the difference in the functional role of the three homologous antiporter-like subunits (NuoN, NuoM, and NuoL).

In the present work, we investigated the functional and structural roles of the charged residues in H^+ translocation in NuoN, together with a few residues in NuoM and NuoL. We also examined the connecting parts in NuoN linking it to the neighboring subunits, accompanied by prolines in the discontinuous helices in NuoN, NuoM, and NuoL. Along with the previous results of mutation studies, the present work highlights similarities and differences among NuoN, NuoM, and NuoL. Furthermore, possible H^+ translocation pathways in the three antiporter-like subunits of the NDH-1 are discussed.

EXPERIMENTAL PROCEDURES

Materials—PCR product, DNA gel extraction, and plasmid purification kits were from Qiagen (Valencia, CA). The pGEM®-T Easy Vector System was from Promega (Madison, WI). The *Taq* DNA polymerase and Rapid DNA Dephos & Ligation Kit were from Roche Applied Science (Indianapolis, IN). The pCRScript cloning kit and the site-directed mutagenesis kit (QuikChange® II XL kit) were from Stratagene (Cedar Creek, TX). The pKO_3 vector was a generous gift from Dr. George M. Church (Harvard Medical School, Boston, MA). The endonucleases were from New England Biolabs (Beverly, MA). *p*-Nitro blue tetrazolium was from EMD Biosciences (La Jolla, CA). The Mini-PROTEAN® TGX™ Precast Gels (4–20%) and Trans-Blot® Turbo™ Transfer Pack were from Bio-Rad. The BCA protein assay kit was from Pierce. Bis-(3-propyl-5-oxo-isoxazol-4-yl)pentamethine oxonol (oxonol VI) and 9-amino-6-chloro-2-methoxyacridine (ACMA) were obtained from Molecular Probes (Eugene, OR). Capsaicin-40 was a generous gift from Dr. Hideto Miyoshi (Kyoto University, Kyoto, Japan). Squamotacin was a generous gift from Dr. Subhash Sinha (The Scripps Research Institute, La Jolla). *n*-Dodecyl β-D-maltoside was from Biosynth International Inc. All other chemicals including dNADH, NADH, and the antibiotics were from Sigma. The antibodies against *E. coli* NDH-1 subunits NuoB, NuoCD, NuoE, NuoF, NuoG, NuoI, NuoK, NuoM, and NuoL were obtained previously in our laboratory (27, 37, 38). Oligonucleotides were synthesized by Valuegene (San Diego, CA). *E. coli* MC4100 (F^-, araD139, Δ(arg F-lac)U169, ptsF25, relA1, flb5301, rpsL 150.λ^-) was used to generate *nuoK*, *NuoL*, *NuoM,* and *NuoN* site-specific mutations.

Preparation of Knock-out and Mutagenesis of the nuoK, nuoL, nuoM, and nuoN Genes in the E. coli Chromosome—The strategies used for generating knock-out mutants ($_N$KO, $_N$E133A/$_K$KO) and mutagenesis of the *E. coli nuoK, nuoL, nuoM,* and *nuoN* genes were in principle similar to those we reported previously (15, 25–30, 39). The knock-out mutants were generated by employing the pKO_3 system according to the method described by Link *et al.* (40) and Kao *et al.* (25) along with minor modifications. In brief, the *spc* gene was inserted into the *nuoN* gene using a HindIII restriction site to disrupt the *nuoN* gene as described in a previous report (27), leading to the construction of the *E. coli* $_N$KO. In parallel, the *nuoN* gene together with a 1-kb DNA segment, both upstream and downstream, was cloned into the pGEM®-T Easy Vector System to generate a template for the site-specific *nuoN* mutations. The mutated *nuoN* fragments were inserted into pKO_3 using the restriction site NotI to construct pKO_3 (*nuoN* mutants). Likewise, stop codons were introduced by the site-directed mutagenesis for the stop mutants ($_N$Val^{469}stop, $_N$Ile^{475}stop, and $_N$Ala^{481}stop). For evaluating the entire process of gene manipulation on the

E. coli chromosome, we also constructed a control mutant ($_N$KO-rev) that employed unmutated gene pKO$_3$(*nouN*), instead of pKO$_3$(*nuoN* mutants), in the recombination process. Then, the above pKO$_3$ plasmids were used to replace the *spc* gene in *E. coli* $_N$KO by recombination. The *E. coli* $_N$E133A/$_K$KO mutant was obtained by transforming pKO$_3$(*nuoK*::*spc*) into the $_N$E133A mutant, and the double mutant $_N$E133A/$_K$E72A was obtained by using pKO$_3$(*nuoK-E72A*) (26). The mutagenesis of *nuoL*, and the *nuoM* gene were done in a similar manner as written in previous reports (24, 27). The point mutations in the chromosome were finally confirmed by direct DNA sequencing.

Growth and Membrane Preparation of E. coli Mutants—*E. coli* cells were grown in Terrific Broth medium at 37 °C until A_{600} of 2. Then inverted membrane vesicles were prepared according to the method described previously in our laboratory (25–27, 30, 41). The membrane preparations were frozen in liquid nitrogen and stored at −80 °C until use.

Immunoblotting and Blue Native Electrophoresis—Fourteen μg of protein from each membrane preparation was first subjected to SDS-PAGE using the discontinuous system of Laemmli (42). The content of the NDH-1 subunits were analyzed by Western blots with antibodies against NuoB (24), NuoCD (39), NuoE, NuoF, NuoG, NuoI (38), NuoK (26), NuoM (27), and NuoL (29) subunits. Blue Native PAGE was performed according to the method of Schägger and von Jagow (43) with some minor modifications. In brief, *E. coli* membranes equivalent to 800 μg of protein were resuspended in 160 μl of 750 mM aminocaproic acid, 50 mM BisTris-HCl (pH 7.0), 0.1 mg/ml of DNase, and 0.5% (w/v) dodecyl maltoside. After incubation and centrifugation, 15-μl samples were analyzed by 4% stacking gel, 7% separating gel. The assembly of NDH-1 was examined by NADH-*p*-nitro blue tetrazolium dehydrogenase activity staining and immunoblotting analysis, using the anti-NuoB antibody as described previously (26, 30, 41).

Enzymatic Assays—The activity assays were conducted according to the methods described previously (44). In brief, dNADH oxidase activity of membrane samples were assayed at 340 nm in 10 mM potassium phosphate buffer (pH 7.0) containing 1 mM EDTA, started by the addition of 0.15 mM dNADH. The dNADH-DB reductase activity measurements were conducted in a similar manner, except that 10 mM KCN and 50 μM DB were also included in the assay mixture. The dNADH-$K_3Fe(CN)_6$ reductase activity was measured in the presence of 10 mM KCN, 150 μM dNADH, and 1 mM $K_3Fe(CN)_6$ at 420 nm in the same buffer. For all assays, at least 3 measurements were made, and the mean ± S.E. calculated.

Measurement of Membrane Potential and H^+-pumping Activity—Generation of membrane potential by the NDH-1 mutants was monitored optically using a reaction mixture containing 0.33 mg/ml of *E. coli* membrane samples in 50 mM MOPS (pH 7.3), 10 mM $MgCl_2$, 50 mM KCl, and 2 μM oxonol VI as described previously (15). The reaction was started by addition of 200 μM dNADH. Uncoupler FCCP was added at a final concentration of 2 μM to dissipate the potential. The H^+ pump activity was followed by ACMA fluorescence quenching (35). Fifty-μg of protein/ml of membrane vesicles, 2 μM ACMA, and 200 μM dNADH were used for the assay. Fluorescence was monitored with excitation at 410 nm and emission at 480 nm on a SpectraMax M2 fluorescence microplate reader (Molecular Devices Corp.).

Other Analytical Procedures—Protein concentrations were determined by the BCA protein assay kit (Pierce) with bovine serum albumin as standard, according to the manufacturer's instructions. Any variations from the procedures and other details are described in the figure legends.

RESULTS

The *E. coli* NuoN subunit (the counterpart of the mitochondrial ND2 subunit) consists of 485 amino acid residues, including 14 transmembrane regions. Fig. 1 shows the deduced amino acid sequence alignment of NuoN from several species spanning from bacteria to human. It also includes NuoL and NuoM of *E. coli* NDH-1 as well as three antiporter-like subunits that are known to be similar to each other. Our previous studies identified conserved charged residues in NuoM ($_M$Glu^{144}, $_M$Lys^{234}, and $_M$Lys^{265}) and NuoL ($_L$Glu^{144}, $_L$Lys^{229}, and $_L$Lys^{399}) that are involved in energy transduction (24, 27). As highlighted in the sequence alignment, NuoN has conserved charged residues at corresponding positions ($_N$Glu^{133}, $_N$Lys^{217}, $_N$Lys^{247}, and $_N$Lys^{395}). Our first aim was to clarify whether these residues are part of the mechanism of H^+ translocation by using a mutagenesis approach (Fig. 2, *blue rectangles*). In addition, to understand the perspective of key residues in NuoL, NuoM, and NuoN, conserved residues that have not been investigated in these subunits, $_M$Glu^{407}, $_L$Arg^{175}, and $_L$Lys^{342}, were also studied.

NuoN, NuoM, and NuoL are known to be structurally similar. One unique feature shared by the three subunits is the presence of two discontinuous helices (17), which were hypothesized to participate in ion translocation. We attempted to elucidate the role of conserved prolines that are located in the loop of those helices (Fig. 2, *orange pentagons*).

Last, the three-dimensional structural model of NDH-1 places residues $_N$Lys^{158} and $_N$His^{224} near helix HL (17). Also, $_N$Val^{469} seems to interact with a β sheet in NuoM. We investigated contributions of these residues to structural integrity of NDH-1 (Fig. 2, *green ovals*).

Conserved Charged Residues in TM in NuoN and Neighboring Subunits—We analyzed *E. coli* membranes on SDS-PAGE by immunoblotting using subunit-specific antibodies (Fig. 3). As expected, membrane vesicles from the knock-out mutants of NuoK, NuoM, and NuoN ($_K$KO, $_M$KO, and $_N$KO) totally lacked all the subunits tested except NuoCD, confirming essential roles of these membrane subunits in the structure of NDH-1. On the other hand, $_L$KO showed the presence of all the tested subunits except for NuoL and NuoM, as reported earlier (29). No detectable differences in the contents of analyzed subunits were seen in the mutants of the conserved charged residues in NuoN and NuoM ($_N$Glu^{133}, $_N$Lys^{217}, $_N$Lys^{247}, $_N$Lys^{395}, and $_M$Glu^{407}). It is important to note that the $_N$KO-rev and $_N$E133A/$_K$KO-rev mutants also showed subunit contents almost comparable with the WT, validating the chromosomal homologous recombination procedure adopted here. On the other hand, the NuoL mutants ($_L$R175A and $_L$K342A) contained considerably

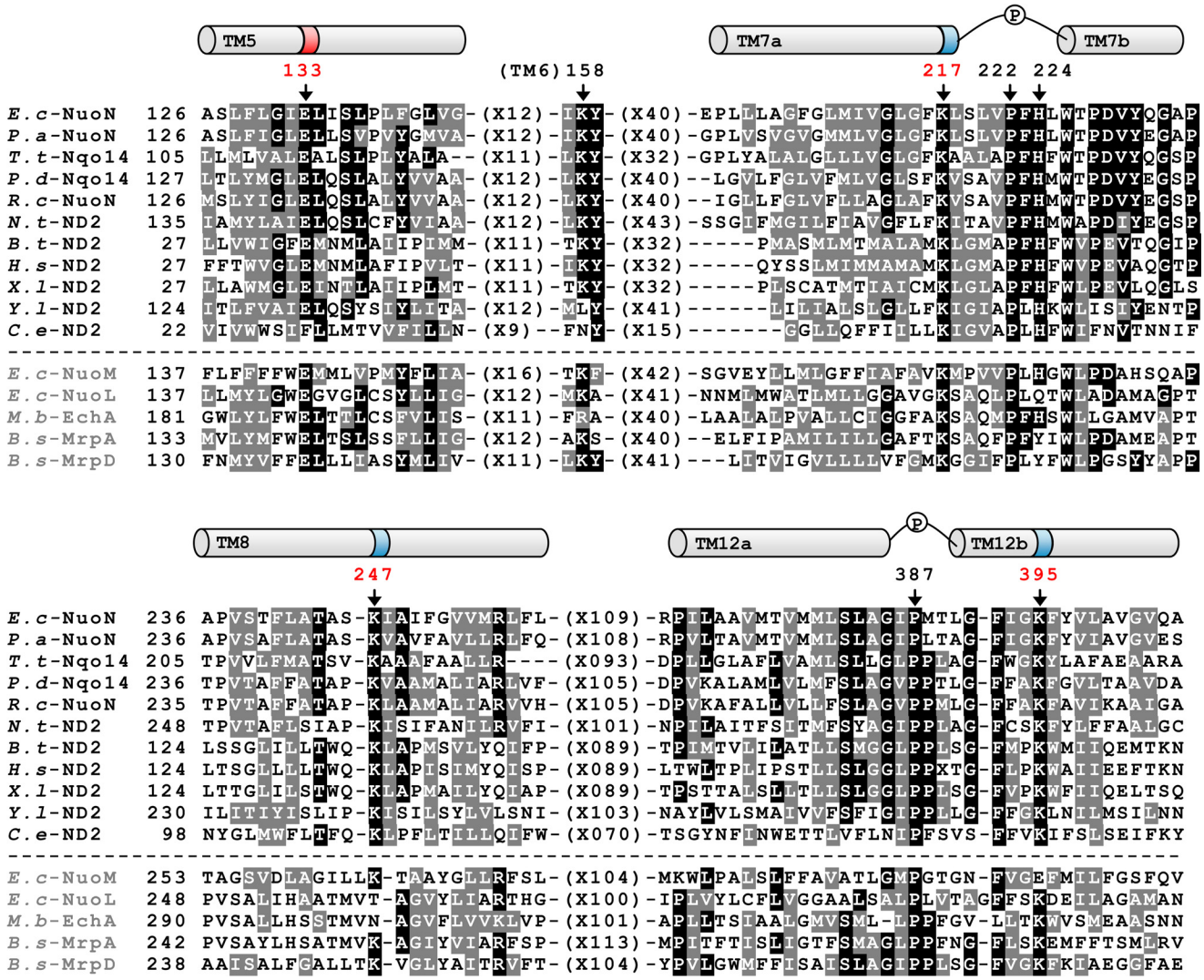

FIGURE 1. **Comparison of the amino acid sequences among the NuoN (ND2) subunits and other homologous antiporters.** The alignment around helices that contain conserved charged residues presumably involved in H^+ translocation was carried out by using the Clustal W program (54). Helices are depicted *above* the alignment based on the three-dimensional structure of *E. coli* NuoN (17), highlighting the candidates of essentially charged residues for energy-coupled NDH-1 activities (*dark colored*) and prolines in discontinuous helices (*P*). *Black boxes with white letters* show identical residues, whereas *dark gray boxes with white letters* illustrate similar residues among at least eight listed organisms. *Dashes* represent gaps to facilitate alignment. Amino acids mutated in this study are marked by *arrows* with the numbering in *E. coli* NuoN. Sequence sources and their UniProtKB/Swiss-Prot accession numbers are: *E.c-NuoN*, *E. coli* K-12 NuoN subunit (P0AFF0); *P.a-NuoN*, *Pseudomonas aeruginosa* NuoN subunit (Q9I0I9); *T.t-Nqo14*, *Thermus thermophilus* Nqo14 subunit (Q56229); *P.d-Nqo14*, *Paraccocus denitrificans* Nqo14 subunit (A1B479); *R.c-NuoN*, *Rhodobacter capsulatus* NuoN subunit (P50973);, *N.t-ND2*, *Nicotiana tabacum* GN Nad2 subunit (Q5MA39); *B.t-ND2*, *Bos taurus* ND2 subunit (P03892); *H.s-ND2*, *Homo sapiens* ND2 subunit (B1NU62); *X.l-ND2*, *Xenopus laevis* ND2 subunit (P03894); *Y.l-ND2*, *Yarrowia lipolytica* ND2 subunit (Q9B6C8);, *C.e-ND2*, *Caenorhabditis elegans* ND2 subunit (P24889); *E.c-NuoM*, *E. coli* K-12 NuoM subunit (P0AFE8); *E.c-NuoL*, *E. coli* K-12 NuoL subunit (P33607); *M.b-EchA*, *Methanosarcina barkeri* EchA subunit (O59652); *B.s-MrpA*, *Bacillus subtilis* MrpA subunit (Q9K2S2); *B.s-MrpD*, *B. subtilis* MrpD subunit (O05229).

lower amounts of NuoL and NuoM in their membranes, suggesting that these mutations make NuoL and NuoM unstable.

The assembly of NDH-1 complex in the mutants was investigated by BN-PAGE followed by NADH dehydrogenase activity staining (Fig. 4*A*). Of the two bands that appeared in the WT membrane, only the upper band was recognized by the antibody to the peripheral subunit NuoB in the immunoblotting of BN-PAGE (Fig. 4*B*). Along with the results from the membrane isolated from the $_N$KO mutant, we regard the upper band as assembled NDH-1. The lower band might be an oligomeric form of NDH-2 but has not been verified. Membranes isolated from the majority of mutants of the charged residues showed a comparable upper band with that from the WT, assuring they contain well assembled NDH-1. On the other hand, mutants $_L$R175A and $_L$K342A exhibited a significantly reduced amount of assembled NDH-1, indicative of partially degraded subcomplexes as reported previously for some other NuoL mutants (24).

In addition to the above analyses, we estimated the amount of the peripheral domain associated with the membrane by measuring the dNADH-$K_3Fe(CN)_6$ reductase activity, which derives from the NADH dehydrogenase segment of NDH-1. Here, we used dNADH as the substrate to eliminate contribution from the alternative NADH-quinone oxidoreductase that exists in *E. coli* (45). As shown in Table 1, $_N$KO and $_N$E133A/$_K$KO mutants exhibited, respectively, only 25 and 20% dNADH-$K_3Fe(CN)_6$ reductase activity as compared to WT, indicating the absence of a functionally active peripheral

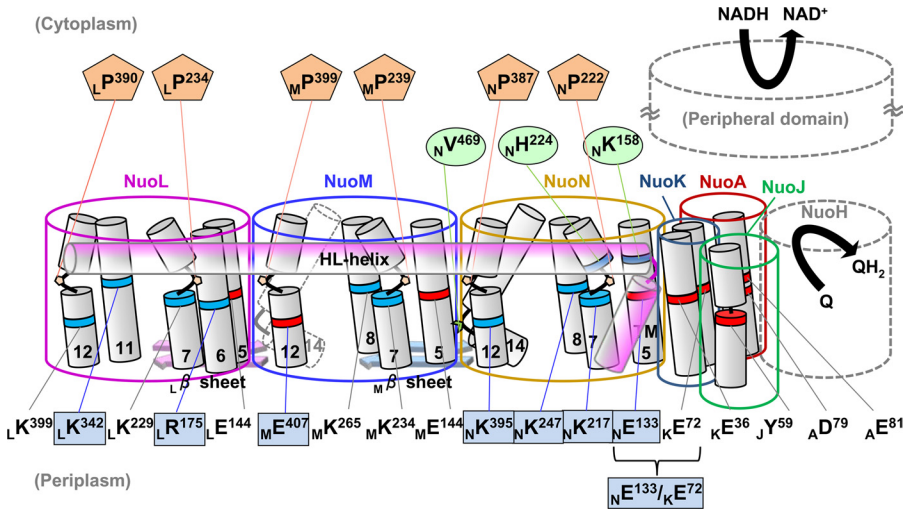

FIGURE 2. **A schematic representation of membrane subunits of *E. coli* NDH-1 illustrating amino acids investigated in this work.** Amino acids proposed to participate in energy transducing activities are listed at the *bottom part*, highlighting residues studied in this paper (*blue rectangles*). NuoN residues involved in connection to the other subunits (*green ovals*) and prolines in the discontinuous helices (TM7 and TM12) in NuoN, NuoM, and NuoL (*orange pentagons*) are listed in the *upper part*. Positively and negatively charged residues are shown in *blue* and *red*, respectively.

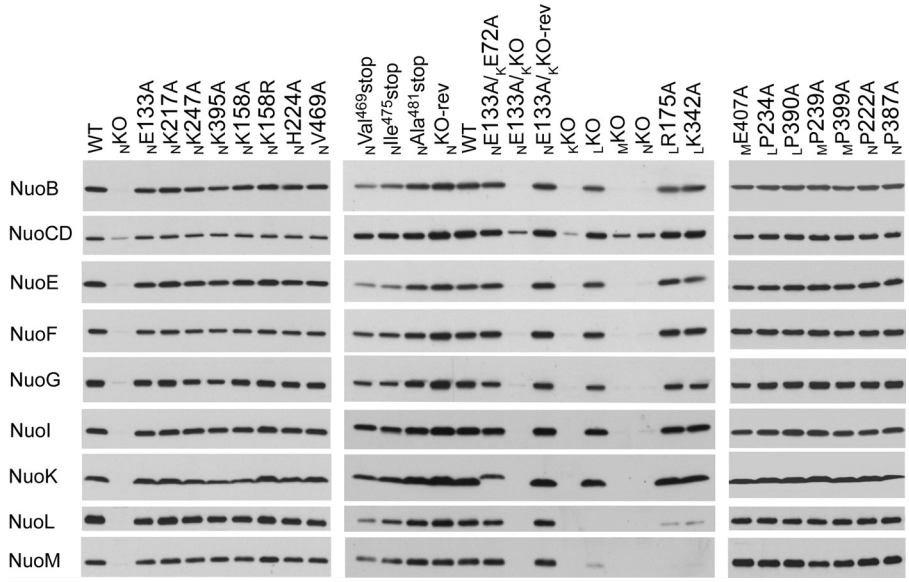

FIGURE 3. **SDS-PAGE and immunoblotting of membrane preparations from NDH-1 mutants.** *E. coli* membranes were loaded on a 4–20% Tris glycine gel. After electrophoresis, the proteins were transferred onto PVDF membranes and Western blotting was carried out. Antibodies specific to NuoB, NuoCD, NuoE, NuoF, NuoG, NuoI, NuoK, NuoL, and NuoM were used.

domain. The residual activities of the two KO mutants were most likely diaphorase activities unrelated to NDH-1 because membranes of KO mutants did not contain NuoF (the NADH-binding subunit) or NuoE that is required for the dNADH-$K_3Fe(CN)_6$ reductase activity of NDH-1 (38, 46). Slight reduction in the activity was seen for some point mutants ($_N$K247A, $_N$K395A, $_M$E407A, $_L$R175A, and $_L$K342A mutants). The remaining single mutants listed in Table 1 exhibited dNADH-$K_3Fe(CN)_6$ reductase activity more or less similar to that of WT.

Next, the dNADH oxidase and dNADH-DB reductase activities were measured to assess the effect of mutations on the energy-coupled activities of NDH-1 (see Table 1). Overall, the dNADH oxidase and dNADH-DB reductase activities behaved in a similar manner among all the mutants tested, implying that the observed effects solely reflect NDH-1 mutations. The mutation of the highly conserved $_N$Glu^{133} to alanine in TM5 showed a small (~28%) decrease in the activities, which is in good agreement with an earlier study by Amarneh and Vik (35). Mutation of the highly conserved $_N$Lys^{217} to alanine, cysteine, or arginine all resulted in reduced activities (in the range of 44–61%). The results are in contrast to that of Amarneh and Vik (35) in which the $_N$K217C mutant was shown to have null energy-coupled activities. The mutation of the other conserved lysine residue to alanine ($_N$K247A) led to only about 30% remaining activity. The mutation of the same residue to arginine resulted in almost complete restoration in the activities similar to the WT. Among the other candidates of essential residues in NuoN, mutation of the highly conserved $_N$Lys^{395} (present in the TM12) to $_N$K395A strikingly caused almost a complete loss in activity, whereas the arginine mutant ($_N$K395R) showed moderately reduced activities in the 37–43% range. When we mutated the highly conserved $_M$Glu^{407} located

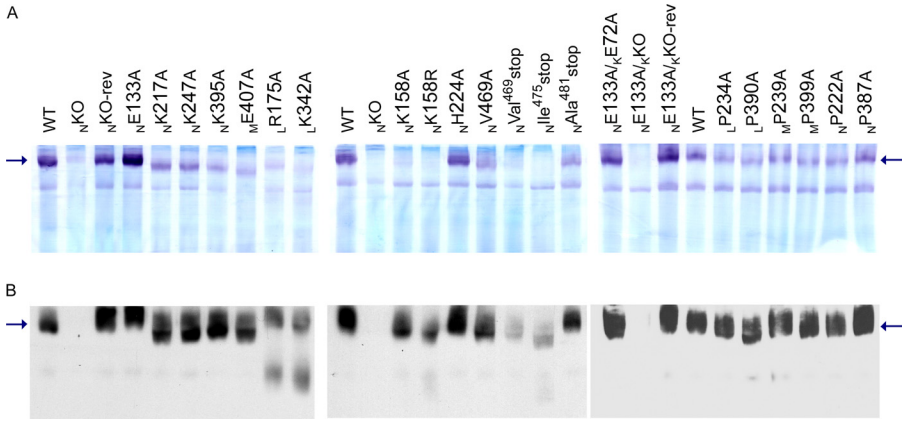

FIGURE 4. **NADH dehydrogenase activity staining (*A*) and immunoblotting (*B*) of BN-PAGE gels of membrane preparations from NDH-1 mutants.** The location of *E. coli* NDH-1 bands is marked by *arrows*. For the extraction of NDH-1 from membrane fractions, 0.5% dodecyl maltoside was used. *A,* for activity staining, the gels were incubated with *p*-nitro blue tetrazolium and NADH. *B,* for immunoblotting, the membrane proteins were electrotransferred onto PVDF membranes after BN-PAGE, and immunostained with the antibody specific to NuoB.

TABLE 1

Conserved charged residues in the TM of NuoN, NuoM, and NuoL potentially involved in energy transduction

Mutation	dNADH-O_2[a]	dNADH-DB[a]	dNADH-$K_3Fe(CN)_6$[b]	IC_{50} (cap)[c]	IC_{50} (squ)[d]
WT	812 ± 25 (100%)	854 ± 37 (100%)	1546 ± 27 (100%)	0.19	0.0023
$_N$KO	5 ± 2 (0.6%)	15 ± 2 (2%)	394 ± 29 (25%)		
$_N$KO-rev	772 ± 74 (95%)	850 ± 81 (100%)	1565 ± 107 (101%)	0.20	0.0061
$_N$E133A	584 ± 42 (72%)	753 ± 136 (88%)	1576 ± 93 (102%)	0.21	0.0040
$_N$E133A/$_K$KO	6 ± 1 (0.7%)	18 ± 2 (2%)	306 ± 56 (20%)		
$_N$E133A/$_K$KO-rev	615 ± 5 (76%)	804 ± 61 (94%)	1497 ± 56 (97%)	0.20	0.0054
$_N$E133A/$_K$E72A	163 ± 15 (20%)	164 ± 5 (19%)	1095 ± 41 (71%)	0.13	0.0029
$_K$KO	(1%)[e]	(7%)[e]	(14%)[e]		
$_K$E72A	(43%)[e]	(48%)[e]	(103%)[e]	0.12[e]	
$_N$K217A	428 ± 42 (53%)	473 ± 61 (55%)	1425 ± 169 (92%)	0.19	0.0030
$_N$K217C	498 ± 53 (61%)	484 ± 24 (57%)	1584 ± 141 (102%)	0.18	0.0052
$_N$K217R	395 ± 37 (49%)	374 ± 27 (44%)	1344 ± 79 (87%)	0.19	0.0038
$_N$K247A	256 ± 21 (32%)	274 ± 24 (32%)	1088 ± 65 (70%)	0.19	0.0028
$_N$K247R	615 ± 91 (76%)	799 ± 110 (94%)	1565 ± 134 (101%)	0.23	0.0043
$_N$K395A	15 ± 2 (2%)	30 ± 3 (4%)	1092 ± 113 (71%)		
$_N$K395R	348 ± 41 (43%)	317 ± 21 (37%)	1397 ± 93 (90%)	0.19	0.0024
$_M$KO	6 ± 2.4 (0.7%)	12 ± 1 (1.4%)	368 ± 23 (24%)		
$_M$E407A	42 ± 5 (5%)	72 ± 10 (8%)	1007 ± 38 (65%)		
$_L$KO	26 ± 4 (3%)	50 ± 8 (6%)	859 ± 120 (56%)		
$_L$R175A	131 ± 8 (16%)	147 ± 7 (17%)	926 ± 10 (60%)	0.17	0.0034
$_L$K342A	92 ± 3 (11%)	94 ± 11 (11%)	968 ± 6 (63%)	0.18	0.0023

[a] Activity in nanomole of dNADH/mg of protein/min.
[b] Activity in nanomole of $K_3Fe(CN)_6$/mg of protein/min.
[c] Concentration of capsaicin-40 (cap) that causes 50% inhibition on dNADH-oxidase activity (μM).
[d] Concentration of squamotacin (squ) that causes 50% inhibition on dNADH-oxidase activity (μM).
[e] From Ref. 26.

in the TM12 (position equivalent to $_N$Lys^{395}) to alanine, almost total abolishment of the activities was observed. Likewise, mutation of the highly conserved charged residues $_L$Arg^{175} and $_L$Lys^{342} to alanine ($_L$R175A and $_L$K342A) resulted in greatly reduced activities (~15%).

To ascertain the effects of the mutations on the energy-coupled activities of NDH-1 further, we examined the generation of membrane potential ($\Delta\Psi$) and H^+ translocation activity. As shown in Fig. 5*A*, addition of dNADH to the membrane vesicles from the WT led to generation of $\Delta\Psi$, which was then dissipated by an uncoupler FCCP. The H^+ translocation activity in the inverted membrane vesicles of different mutants was monitored by ACMA, where the membranes from the WT showed a maximum quenching after the addition of dNADH, followed by a reversion of the signal when FCCP was added (Fig. 6*A*). The mutation of highly conserved $_M$Glu^{407} and $_N$Lys^{395} to alanine resulted in a significant loss in $\Delta\Psi$ generation and no H^+ pumping activity (only ~10% as compared with the WT). Those of $_L$R175A and $_L$K342A exhibited only a small $\Delta\Psi$ generation and H^+ pumping activity (~30%). In contrast, other mutants of highly conserved residues including $_N$E133A, $_N$K217A, and $_N$K247A exhibited $\Delta\Psi$ and H^+ pumping activity almost comparable with that of the WT. These results were largely consistent with the data of the energy-coupled activities.

In good agreement with an earlier report (35), our present results relating to the conserved charged residues on the NuoN subunit showed that $_N$Lys^{395} located in the TM12 is an essential residue for the energy-transducing NDH-1 activity. $_N$Lys^{395} is also conserved in NuoL ($_L$Lys^{399}) but in the homologous NuoM subunit the equivalent residue is a glutamic acid ($_M$Glu^{407}). Our studies demonstrated that both $_L$Lys^{399} (24) and $_M$Glu^{407} (this work, see Table 1 and Figs. 5 and 6) are essential residues. As depicted in Fig. 7*A*, the three-dimensional structure of NDH-1 indicates that $_M$Glu^{407} interacts with the essential residue $_L$Arg^{175}, whereas $_N$Lys^{395} interacts with the essential residue

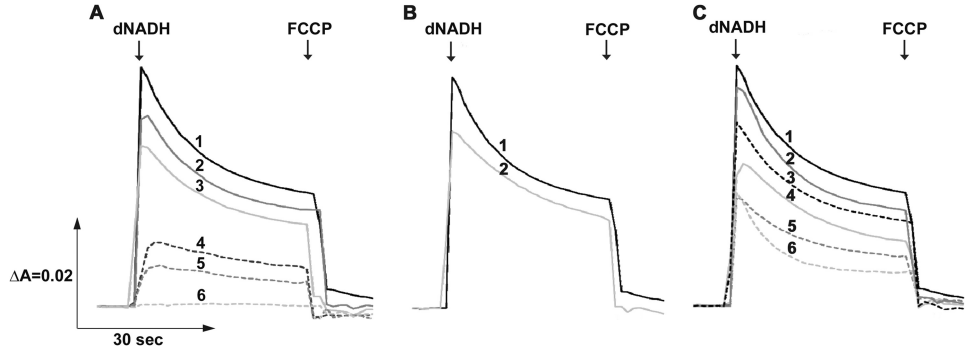

FIGURE 5. **Detection of the membrane potential generated by dNADH oxidation in NDH-1 mutants.** The potential changes ($\Delta\Psi$) of *E. coli* membrane samples were monitored by the absorbance changes of oxonol VI at 630–603 nm at 30 °C. The *first arrow* indicates addition of dNADH, whereas the *second arrow* indicates addition of FCCP. Representative traces from different groups of mutants: *A,* conserved charged residue mutants: **1**, WT (or $_N$KO-rev, $_N$E133A, $_N$E133A/$_K$KO-rev, $_N$K217C, and $_N$K247R); **2**, $_N$K217A (or $_N$K217R); **3**, $_N$K247A (or $_N$K395R); **4**, $_L$R175A (or $_L$K342A and $_L$KO); **5**, $_N$K395A (or $_M$E407A and $_N$E133A/$_K$E72A); **6**, $_N$KO (or $_N$E133A/$_K$KO); *B,* conserved proline mutants: **1**, WT (or $_N$P387G); **2**, $_N$P222A (or $_N$P387A, $_M$P239A, $_M$P399A, $_L$P234A, and $_L$P390A); and *C,* structural element residues: **1**, WT; **2**, $_N$K158A (or $_N$H224A and $_N$V469A); **3**, $_N$Ala^{481}stop; **4**, $_N$K158R; **5**, $_N$Ile^{475}stop; **6**, $_N$Val^{469}stop.

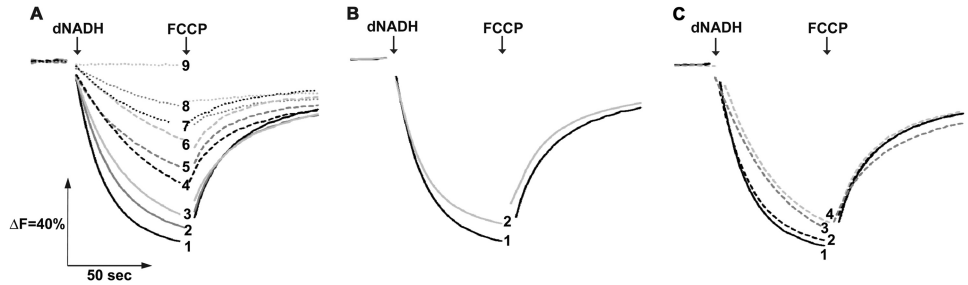

FIGURE 6. **Generation of a pH gradient coupled to dNADH oxidation in NDH-1 mutants.** H^+ translocations of *E. coli* membrane samples were measured by the quenching of ACMA fluorescence at room temperature with an excitation wavelength of 410 nm and an emission wavelength of 480 nm. Addition of dNADH or FCCP is indicated by the *arrows*. Representative traces from different group of mutants: *A,* conserved charged residue mutants: **1**, WT (or $_N$KO-rev, $_N$E133A, $_N$E133A/$_K$KO-rev, $_N$K217C and $_N$K247R); **2**, $_N$K217*A*; **3**, $_N$K247A (or $_N$K217R and $_N$K395R); **4**, $_L$R175A (or $_L$K342A); **5**, $_N$E133A/$_K$E72A; **6**, $_L$KO; **7**, $_M$E407A; **8**, $_N$K395A; **9**, $_N$KO (or $_N$E133A/$_K$KO); *B,* conserved proline mutants: **1**, WT (or $_N$P387G); **2**, $_N$P222A (or $_N$P387A, $_M$P239A, $_M$P399A, $_L$P234A, and $_L$P390A); and *C,* structural element residues: **1**, WT; **2**, $_N$K158A (or $_N$H224A, $_N$V469A and $_N$Ala^{481}stop); **3**, $_N$K158R (or $_N$Ile^{475}stop); **4**, $_N$Val^{469}stop.

$_M$Glu^{144} (27), rationalizing the necessity of the opposite charges between $_N$Lys^{395} and $_M$Glu^{407}.

The conserved residue $_N$Glu^{133} was seemingly non-essential for the energy-transducing NDH-1 activity unlike the corresponding glutamic residues in NuoM and NuoL ($_M$Glu^{144} and $_L$Glu^{144}) that had been shown to be essential (24, 27, 28, 36). According to the three-dimensional structural model of NDH-1, another conserved but non-essential residue $_K$Glu^{72} (26) is located close to $_N$Glu^{133} (4.06 Å). Thus, we investigated a possible interaction between these two carboxyl residues by mutation analysis involving the $_N$E133A/$_K$E72A double mutant.

As shown in Fig. 3, the subunit contents of the $_N$E133A/$_K$E72A mutant were comparable with that of the WT, with slightly slower migration of the NuoK subunit as reported for $_K$E72A in our earlier study (26). Although slight reduction in the dNADH-$K_3Fe(CN)_6$ reductase activity was seen for the $_K$E72A/$_N$E133A mutant (Table 1), the membrane isolated from the double mutant seemed to contain similar amounts of fully assembled NDH-1 (Fig. 4). Thus, it appeared that the possible interaction of the two glutamic acids is not critical for the connection of the NuoN and NuoK subunits. On the other hand, the double mutation of $_K$Glu^{72} and $_N$Glu^{133} ($_N$E133A/$_K$E72A) strongly reduced energy-coupled activities (20%), whereas the activities of single mutants $_N$E133A (this work) and $_K$E72A (from (26)) were about 80 and 45%, respectively. Accordingly, the strong reduction of $\Delta\Psi$ and H^+ translocation activity of the double mutant were observed (Figs. 5*A* and 6*A*).

These results suggest an essential role of the pair of these two highly conserved glutamic acids on the energy-coupled NDH-1 activity. Thus we postulate that $_N$Glu^{133} is important for function similarly to the corresponding residues in NuoM and NuoL ($_M$Glu^{144} and $_L$Glu^{144}) but its role can be compensated by another residue, $_K$Glu^{72}. It should also be noted that a compensatory effect exerted by two conserved charged residues has been reported for the two nearby conserved carboxyl residues ($_A$Asp^{79} and $_A$Glu^{81}) located in the NuoA subunit (25) but never for a pair of residues located in different subunits like in the current case. These results strongly suggest that NuoN has function of the H^+ translocation like NuoM and NuoL.

Prolines in Discontinuous Helices of Subunits NuoN, NuoM, and NuoL—It has recently been demonstrated that discontinuous membrane helices (α-helix–loop–α-helix motif) are present in Ca^{2+}-ATPase and secondary transporters such as NhaA (47). The three-dimensional structural models of these transporters led to a hypothesis that the loops are involved in recognition, binding, and translocation of ions. Similar to the secondary antiporters (17), NuoN, NuoM, and NuoL all have two discontinuous helices in their TM7 and TM12 sections, which are located close to essential charged residues, thus implying a key role for conformational changes in these subunits (see Figs. 2 and 7*B*). As highly conserved prolines are located at the bend-

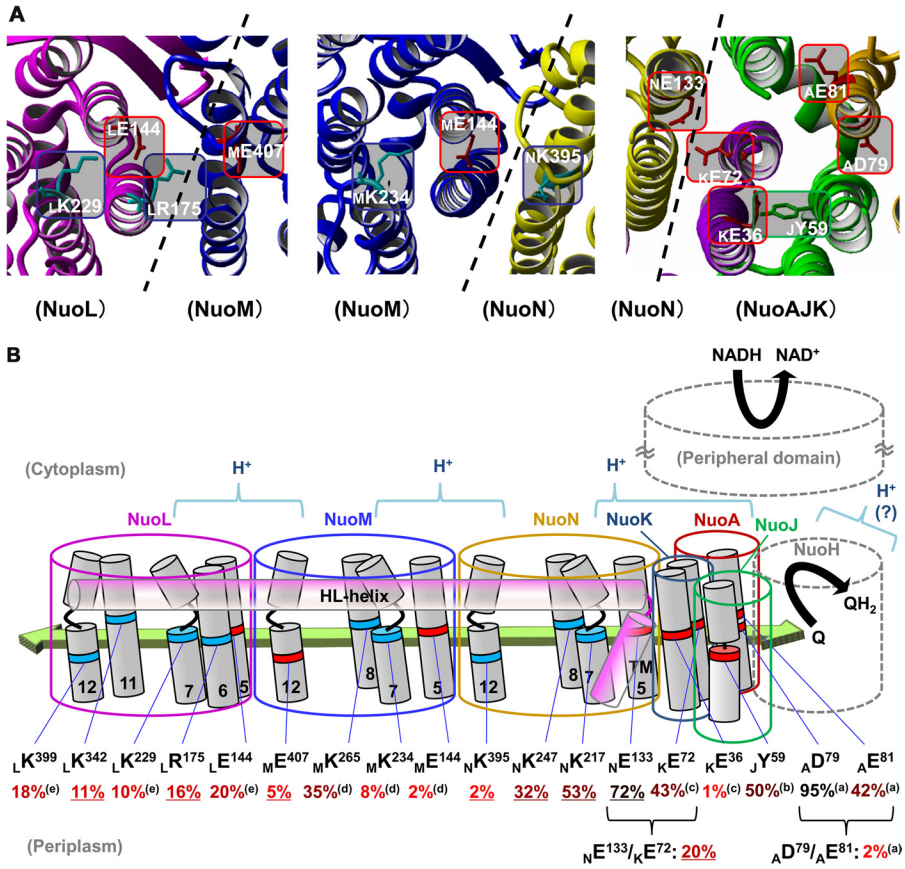

FIGURE 7. **A schematic representation of the membrane domain of *E. coli* NDH-1 highlighting the candidates of charged residues involved in energy-coupled NDH-1 activity.** *A,* schematics depicting the charged residues at the borders among the membrane subunits. The three-dimensional structure in *ribbon* was drawn from the coordinate file 3RKO using YASARA version 11.11.2. *B,* a schematic drawing of membrane subunits displaying their charged residues possibly involved in energy-coupled NDH-1 activity, in *red* for negatively charged and *blue* for positively charged residues, respectively. The postulated conformational change driven by horizontal electrochemical transmission among charged residues is illustrated with a *green arrow* and possible core regions for H^+ translocation are indicated with *blue case arcs*. *E. coli* numbering is displayed in *parentheses*. The dNADH-oxidase activity of alanine mutants (except $_J$Tyr^{59} which was mutated to Phe) compared with the WT are shown (in %), listed from Tables 1–3 (*underlined*) and previous reports: *a, Ref.* 25; *b*, Ref. 41; *c*, Ref. 26; *d*, Ref. 27; *e*, Ref. 24, highlighting significant decreases in the activities in *bright red*.

ing of the discontinuous helices in NDH-1 ($_N$Pro^{222}, $_N$Pro^{387}, $_M$Pro^{239}, $_M$Pro^{399}, $_L$Pro^{234}, and $_L$Pro^{390}) (Fig. 2), replacing them with alanine, which is a strong α-helix-forming residue, might possibly force the helices into a less kinked structure. Therefore, we made mutations $_N$P222A, $_N$P387A, $_M$P239A, $_M$P399A, $_L$P234A, and $_L$P390A, along with a glycine mutant $_N$P387G.

The analysis of SDS-PAGE (Fig. 3), BN-PAGE (Fig. 4), and dNADH-$K_3Fe(CN)_6$ reductase activity (Table 2) confirm that all of the proline mutants had normal subunit contents and assembly. As expected, mutation of each of the conserved prolines to alanine moderately reduced the dNADH oxidase and the dNADH-DB reductase activities (50–80%, Table 2). Likewise, these mutants gave a slight reduction of $\Delta\Psi$ and H^+ translocation (Figs. 5*B* and 6*B*). The energy-coupled activities of a mutation of $_N$Pro^{387} to glycine ($_N$P387G) as well as the extent of $\Delta\Psi$ and H^+ translocation were comparable with WT, suggesting that replacement with glycine, which has no side chain and is thus relatively flexible, perhaps did not deprive the helix of kink enough to cause a significant activity loss.

The remaining activities of mutation of the prolines to alanine indicated their similar roles among the antiporter-like subunits. However, their relatively high activities do not seem to support the hypothesis (17) that the individual proline residues are indispensable for the energy-coupled NDH-1 activities. It might be possible that replacement of a proline residue by alanine in a different discontinuous helix only partially affects the kinked structure of NDH-1. In addition, we could not exclude a possibility that discontinuous helices do not make a significant contribution to the energy coupling mechanism.

Structural Elements in NuoN—The x-ray structure of *E. coli* NDH-1 displayed at least two connection elements among NuoK, NuoN, NuoM, and NuoL, which are considered to contribute to the stability of the antiporter-like subunits and help in coupling electron transfer with H^+ translocation (17, 29, 48, 49). One is a rod-like helix HL in NuoL, and the other is β sheets in NuoL and NuoM located on the opposite side of the domain from helix HL (17) (Fig. 2). In NuoN subunit, residues $_N$Lys^{158} and $_N$His^{224} are placed near helix HL according to the x-ray structural model. Also, $_N$Val^{469} (or the α-helix in $_N$TM14 from $_N$Val^{469} to the C-terminal) seem to interact with the $_M\beta$ sheet.

We investigated the possible connecting elements ($_N$Lys^{158} and $_N$His^{224}) of NuoN with the helix HL in NuoL by producing mutants $_N$K158A, $_N$K158R, and $_N$H224A. When we measured dNADH oxidase and dNADH-DB reductase activities, a mod-

TABLE 2
Conserved prolines located in the loops of discontinuous helices of NuoN, NuoM, and NuoL

Mutation	dNADH-O_2[a]	dNADH-DB[a]	dNADH-$K_3Fe(CN)_6$[b]	IC_{50} (cap)[c]	IC_{50} (squ)[d]
WT	812 ± 25 (100%)	854 ± 37 (100%)	1546 ± 27 (100%)	0.19	0.0023
$_N$P222A	503 ± 21 (62%)	655 ± 15 (77%)	1400 ± 19 (91%)	0.20	0.0027
$_N$P387A	479 ± 31 (59%)	442 ± 14 (52%)	1285 ± 34 (83%)	0.19	0.0023
$_N$P387G	705 ± 65 (87%)	780 ± 56 (91%)	1594 ± 60 (103%)	0.18	0.0028
$_M$P239A	477 ± 14 (59%)	621 ± 17 (73%)	1343 ± 50 (87%)	0.18	0.0047
$_M$P399A	422 ± 28 (52%)	540 ± 12 (63%)	1204 ± 87 (78%)	0.20	0.0044
$_L$P234A	422 ± 15 (52%)	569 ± 46 (67%)	1315 ± 67 (85%)	0.16	0.0025
$_L$P390A	485 ± 35 (60%)	578 ± 65 (68%)	1399 ± 51 (90%)	0.15	0.0030

[a] Activity in nanomole of dNADH/mg of protein/min.
[b] Activity in nanomole of $K_3Fe(CN)_6$/mg of protein/min.
[c] Concentration of capsaicin-40 (cap) that causes 50% inhibition on dNADH-oxidase activity (μM).
[d] Concentration of squamotacin (squ) that causes 50% inhibition on dNADH-oxidase activity (μM).

erate decrease was observed for $_N$K158A and $_N$K158R mutants (~50%, Table 3). The $_N$H224A mutant displayed a slight decrease in the energy-coupled activities (~70%). Similarly, $\Delta\Psi$ and the H^+ translocation activity were only slightly reduced by these mutations (Figs. 5*C* and 6*C*). Interestingly, mutants $_N$K158A and $_N$K158R showed significantly decreased levels of the intact NDH-1 activity on BN-PAGE (Fig. 4*A*) despite the detection of fully assembled NDH-1 as seen in immunoblotting (Fig. 4*B*), the normal subunit contents (Fig. 3) and the dNADH-$K_3Fe(CN)_6$ reductase activity (Table 3). This discrepancy might be due to the extraction procedures in BN-PAGE, which requires dissociation of the membrane using dodecyl maltoside as described previously (26). The loss of connecting residue $_N$Lys^{158} could reduce the stability of helix HL resulting in an altered architecture in that part of NDH-1. Along with the three-dimensional structural model of membrane subunits, these results strongly suggested that $_N$Lys^{158} plays a critical role in the interaction with helix HL. On the other hand, alanine mutation of the conserved histidine residues, $_M$His^{241} (27) and $_N$His^{224} (this work), seemed to imply that their involvement in the interaction with helix HL may be less significant compared with that of $_N$Lys^{158}.

To assess the other possible connecting element ($_N$Val^{469}) in the NuoN subunit, we also made the mutation and truncations of the NuoN subunit ($_N$V469A, $_N$Val^{469}stop, $_N$Ile^{475}stop, and $_N$Ala^{481}stop). The amount of membrane and peripheral subunits were reduced for the C-terminal truncation $_N$Val^{469}stop and $_N$Ile^{475}stop mutants (Fig. 3). In contrast, the truncation mutant $_N$Ala^{481}stop and a point mutant $_N$V469A showed subunit contents mostly comparable with that of the WT. We also found a reduced amount of completely assembled NDH-1 in BN-PAGE (Fig. 4) and partially reduced dNADH-$K_3Fe(CN)_6$ reductase activities (60%, Table 3) for the $_N$Val^{469}stop and $_N$Ile^{475}stop mutants. In line with the above analysis, $_N$Val^{469}stop or $_N$Ile^{475}stop mutants displayed a significant decrease in the energy-coupled NDH-1 activities (~30%), whereas the $_N$Ala^{481}stop and $_N$V469A mutants showed relatively higher activities (~65%). The data on $\Delta\Psi$ generation and H^+ translocation ability exhibited similar tendencies with the energy-coupled activities (Figs. 5*C* and 6*C*). These results indicated that the C-terminal amphipathic helix starting from $_N$Val^{469} in $_N$TM14 interacts with the $_M\beta$ sheet. Interestingly, the loss of NuoL and NuoM in NDH-1 was detected in C-terminal truncation mutants of NuoM (29) but not in the C-terminal truncation mutants of NuoN.

Effect of Inhibitors on the Energy-coupled NDH-1 Activities—Capsaicin-40 is a competitive inhibitor for quinone and inhibits the energy-coupled activities in NDH-1 (50, 51). No significant difference in the IC_{50} values for capsaicin-40 (0.13–0.23 μM) was found among the WT and the mutants analyzed in this work (Tables 1–3). A complex I specific inhibitor, squamotacin (one of acetogenins), showed strong inhibition for the majority of the mutants constructed in this work. The IC_{50} value of squamotacin (2.3–6.1 nM) was similar to that of another acetogenin, asimicin, which was described to have the best inhibitory potency against *E. coli* NDH-1 (24). These results exemplify that all residues studied in this work do not contribute to construction of the quinone-binding site or inhibitor-binding site(s), in line with the x-ray structural model (19).

DISCUSSION

Based on the empirical findings in this study, we concluded that NuoN is involved in H^+ translocation similar to the other antiporter-like subunits, NuoM and NuoL. Our data also suggested that $_N$Glu^{133} and $_N$Lys^{395} in NuoN may be involved in H^+ translocation. Together with the results from our previous work, we summarized the candidate residues that may be part of the mechanism of H^+ translocation as shown in Fig. 7*B*. Besides the aforementioned residues in NuoN, they are $_K$Glu^{36}, $_M$Glu^{144}, $_M$Lys^{234}, $_M$Glu^{407}, $_L$Glu^{144}, $_L$Arg^{175}, $_L$Lys^{229}, $_L$Lys^{342}, and $_L$Lys^{399}. In addition, $_A$Asp^{79}, $_A$Glu^{81}, and $_K$Glu^{72} were also considered to be essential residues based on the data using the double mutants. Most of the residues are located not only in the middle of the TM but also at the interface of adjacent subunits, suggesting that the core elements of the H^+ translocation machinery lie around the borders of contiguous membrane domain subunits (52). Recently, Verkhovskaya and Bloch (53) proposed a "wave-spring" model that involves conformational changes driven by the reduction of quinone transmitted through charged residues located in the middle of the TMs, from the NuoAJK(H) bundle to NuoL. In this model, electrochemical transmission has to cover the distance between the two closest charged residues. There exist large gaps around the border of subunits, especially between TM8 and TM12. Sazanov's group (19) suggested a "river" of water molecules and histidine residues that assist formation of a continuous hydrophilic axis in the membrane (see the *green arrow* in Fig. 7*B*). Therefore, it is possible that replacements of the charged residues by site-directed mutagenesis at the interface of adjacent subunits had a critical impact on energy-

TABLE 3
Residues interacting with helix HL and β-sheets

Mutation	dNADH-O_2[a]	dNADH-DB[a]	dNADH-$K_3Fe(CN)_6$[b]	IC_{50} (cap)[c]	IC_{50} (squ)[d]
WT	812 ± 25 (100%)	854 ± 37 (100%)	1546 ± 27 (100%)	0.19	0.0023
$_N$K158A	408 ± 45 (50%)	489 ± 54 (57%)	1224 ± 16 (79%)	0.18	0.0028
$_N$K158R	330 ± 43 (41%)	350 ± 60 (41%)	1155 ± 127 (75%)	0.13	0.0022
$_N$H224A	567 ± 65 (70%)	623 ± 49 (73%)	1391 ± 92 (90%)	0.15	0.0032
$_N$V469A	504 ± 52 (62%)	612 ± 52 (72%)	1358 ± 95 (88%)	0.15	0.0031
$_N$Val^{469}stop	299 ± 13 (37%)	354 ± 12 (41%)	970 ± 87 (63%)	0.18	0.0031
$_N$Ile^{475}stop	307 ± 9 (38%)	237 ± 39 (28%)	923 ± 88 (60%)	0.14	0.0032
$_N$Ala^{481}stop	505 ± 31 (62%)	575 ± 28 (67%)	1267 ± 37 (82%)	0.15	0.0025

[a] Activity in nanomole of dNADH/mg of protein/min.
[b] Activity in nanomole of $K_3Fe(CN)_6$/mg of protein/min.
[c] Concentration of capsaicin-40 (cap) that causes 50% inhibition on dNADH-oxidase activity (μM).
[d] Concentration of squamotacin (squ) that causes 50% inhibition on dNADH-oxidase activity (μM).

coupled activities because of the gaps with adjacent charged residues. Thus, H^+ can be translocated through the inside of the antiporter-like subunits (NuoL, NuoM, and NuoN) and also through the aforementioned NuoAJK(H) bundle, powered by the horizontal array of charged/polar groups in conjunction with conformational changes in different membrane subunits (Fig. 7*B*).

We categorized three areas/regions of essential charged residues that could comprise the key elements in the H^+ translocation pathway (see Fig. 7*A*). They are: 1) a negatively charged region formed by essential residues $_N$Glu^{133}, $_K$Glu^{72}, $_K$Glu^{36}, $_A$Glu^{81}, and $_A$Asp^{79} in the NuoAJKN bundle; 2) a positively and negatively charged area around the border between NuoN and NuoM formed by $_N$Lys^{395}, $_M$Glu^{144}, and $_M$Lys^{234}; and 3) a positively and negatively charged region around the border between NuoM and NuoL formed by $_M$Glu^{407}, $_L$Arg^{175}, $_L$Glu^{144}, and $_L$Lys^{229}. Both points 2 and 3 consist of a combination of positively and negatively charged residues, suggesting that their ionic interaction could play a central role in energy transmission, rather than a mere ionic connection as none of the mutants of the aforementioned residues caused any drastic change in the assembly of NDH-1 (except for certain residues in NuoL). In addition, there are additional possibilities for core parts of H^+ translocation pathways in the positively charged region near the end of NuoL formed by conserved residues, $_L$Lys^{342} and $_L$Lys^{399}, and/or in subunit NuoH (19). Along with the fact that the set of $_N$Glu^{133} and $_K$Glu^{72} are the propensity of essential charged residues (whose double mutations led to a significant loss of activity) to be located at the interface of adjacent subunits, it seems reasonable to imagine that H^+ translocation occurs through the interface between two adjacent subunits, as shown in Fig. 7*B*. Our results on the site-directed mutagenesis suggest that $_L$Lys^{342} and $_L$Lys^{399} are also involved in the maintenance of architecture of NDH-1. From the mutation experiments on NuoL, $_L$Asp^{400} (adjacent to $_L$Lys^{399}) was considered to be involved in H^+ translocation (24). Further research would help establish whether this region participates in H^+ translocation and/or structural stability of NDH-1.

In conclusion, the results of the present study suggested that (*a*) the NuoN subunit is involved in the H^+ translocation in a similar manner to NuoM and NuoL, (*b*) conserved chargeable residues including those at the interface of adjacent subunits play key roles in the mechanism of H^+ translocation, as the requisites for horizontal energy transmission and/or H^+ translocation pathways, (*c*) conserved prolines in the loops of discontinuous helices are not essential for the energy transduction of NDH-1, and (*d*) a lysine residue and the C terminus region in NuoN bear structural roles.

Acknowledgments—We thank Drs. Mathieu Marella and Gaurav Patki for discussion, Dr. Jennifer Barber-Singh for critical reading of the manuscript, Dr. Hideto Miyoshi for providing capsaicin 40, and Dr. Subhash Sinha for squamotacin.

REFERENCES

1. Brandt, U. (2006) Energy converting NADH:quinone oxidoreductase (complex I). *Annu. Rev. Biochem.* **75,** 69–92
2. Wikström, M., and Hummer, G. (2012) Stoichiometry of proton translocation by respiratory complex I and its mechanistic implications. *Proc. Natl. Acad. Sci. U.S.A.* **109,** 4431–4436
3. Carroll, J., Fearnley, I. M., Skehel, J. M., Shannon, R. J., Hirst, J., and Walker, J. E. (2006) Bovine complex I is a complex of forty-five different subunits. *J. Biol. Chem.* **281,** 32724–32727
4. Sharma, L. K., Lu, J., and Bai, Y. (2009) Mitochondrial respiratory complex I. Structure, function and implication in human diseases. *Curr. Med. Chem.* **16,** 1266–1277
5. Yagi, T., Yano, T., Di Bernardo, S., and Matsuno-Yagi, A. (1998) Procaryotic complex I (NDH-1), an overview. *Biochim. Biophys. Acta* **1364,** 125–133
6. Yagi, T., and Matsuno-Yagi, A. (2003) The proton-translocating NADH-quinone oxidoreductase in the respiratory chain. The secret unlocked. *Biochemistry* **42,** 2266–2274
7. Efremov, R. G., Baradaran, R., and Sazanov, L. A. (2010) The architecture of respiratory complex I. *Nature* **465,** 441–445
8. Yagi, T., and Dinh, T. M. (1990) Identification of the NADH-binding subunit of NADH-ubiquinone oxidoreductase of *Paracoccus denitrificans*. *Biochemistry* **29,** 5515–5520
9. Yano, T., and Yagi, T. (1999) H^+-translocating NADH-quinone oxidoreductase (NDH-1) of *Paracoccus denitrificans.* Studies on topology and stoichiometry of the peripheral subunits. *J. Biol. Chem.* **274,** 28606–28611
10. Berrisford, J. M., and Sazanov, L. A. (2009) Structural basis for the mechanism of respiratory complex I. *J. Biol. Chem.* **284,** 29773–29783
11. Hinchliffe, P., and Sazanov, L. A. (2005) Organization of iron-sulfur clusters in respiratory complex I. *Science* **309,** 771–774
12. Yakovlev, G., Reda, T., and Hirst, J. (2007) Reevaluating the relationship between EPR spectra and enzyme structure for the iron sulfur clusters in NADH:quinone oxidoreductase. *Proc. Natl. Acad. Sci. U.S.A.* **104,** 12720–12725
13. Ohnishi, T., and Nakamaru-Ogiso, E. (2008) Were there any "misassignments" among iron-sulfur clusters N4, N5 and N6b in NADH-quinone oxidoreductase (complex I)? *Biochim. Biophys. Acta* **1777,** 703–710
14. Sazanov, L. A. (2007) Respiratory complex I. Mechanistic and structural insights provided by the crystal structure of the hydrophilic domain. *Bio-*

chemistry **46,** 2275–2288
15. Sinha, P. K., Nakamaru-Ogiso, E., Torres-Bacete, J., Sato, M., Castro-Guerrero, N., Ohnishi, T., Matsuno-Yagi, A., and Yagi, T. (2012) Electron transfer in subunit NuoI (TYKY) of *Escherichia coli* NDH-1 (NADH:quinone oxidoreductase). *J. Biol. Chem.* **287,** 17363–17373
16. Shiraishi, Y., Murai, M., Sakiyama, N., Ifuku, K., and Miyoshi, H. (2012) Fenpyroximate binds to the interface between PSST and 49 kDa subunits in mitochondrial NADH-ubiquinone oxidoreductase. *Biochemistry* **51,** 1953–1963
17. Efremov, R. G., and Sazanov, L. A. (2011) Structure of the membrane domain of respiratory complex I. *Nature* **476,** 414–420
18. Hunte, C., Zickermann, V., and Brandt, U. (2010) Functional modules and structural basis of conformational coupling in mitochondrial complex I. *Science* **329,** 448–451
19. Baradaran, R., Berrisford, J. M., Minhas, G. S., and Sazanov, L. A. (2013) Crystal structure of the entire respiratory complex I. *Nature* **494,** 443–448
20. Mathiesen, C., and Hägerhäll, C. (2002) Transmembrane topology of the NuoL, M and N subunits of NADH:quinone oxidoreductase and their homologues among membrane-bound hydrogenases and bona fide antiporters. *Biochim. Biophys. Acta* **1556,** 121–132
21. Kajiyama, Y., Otagiri, M., Sekiguchi, J., Kudo, T., and Kosono, S. (2009) The MrpA, MrpB, and MrpD subunits of the Mrp antiporter complex in *Bacillus subtilis* contain membrane-embedded and essential acidic residues. *Microbiology* **155,** 2137–2147
22. Hedderich, R. (2004) Energy-converting [NiFe] hydrogenases from archaea and extremophiles. Ancestors of complex I. *J. Bioenerg. Biomembr.* **36,** 65–75
23. Mathiesen, C., and Hägerhäll, C. (2003) The "antiporter module" of respiratory chain Complex I includes the MrpC/NuoK subunit. A revision of the modular evolution scheme. *FEBS Lett.* **549,** 7–13
24. Nakamaru-Ogiso, E., Kao, M. C., Chen, H., Sinha, S. C., Yagi, T., and Ohnishi, T. (2010) The membrane subunit NuoL(ND5) is involved in the indirect proton pumping mechanism of *E. coli* complex I. *J. Biol. Chem.* **285,** 39070–39078
25. Kao, M. C., Di Bernardo, S., Perego, M., Nakamaru-Ogiso, E., Matsuno-Yagi, A., and Yagi, T. (2004) Functional roles of four conserved charged residues in the membrane domain subunit NuoA of the proton-translocating NADH-quinone oxidoreductase from *Escherichia coli*. *J. Biol. Chem.* **279,** 32360–32366
26. Kao, M. C., Nakamaru-Ogiso, E., Matsuno-Yagi, A., and Yagi, T. (2005) Characterization of the membrane domain subunit NuoK (ND4L) of the NADH-quinone oxidoreductase from *Escherichia coli*. *Biochemistry* **44,** 9545–9554
27. Torres-Bacete, J., Nakamaru-Ogiso, E., Matsuno-Yagi, A., and Yagi, T. (2007) Characterization of the NuoM (ND4) subunit in *Escherichia coli* NDH-1. Conserved charged residues essential for energy-coupled activities. *J. Biol. Chem.* **282,** 36914–36922
28. Torres-Bacete, J., Sinha, P. K., Castro-Guerrero, N., Matsuno-Yagi, A., and Yagi, T. (2009) Features of subunit NuoM (ND4) *Escherichia coli* NDH-1. Topology and implication of conserved Glu-144 for coupling site 1. *J. Biol. Chem.* **284,** 33062–33069
29. Torres-Bacete, J., Sinha, P. K., Matsuno-Yagi, A., and Yagi, T. (2011) Structural contribution of C-terminal segments of NuoL (ND5) and NuoM (ND4) subunits of complex I from *Escherichia coli*. *J. Biol. Chem.* **286,** 34007–34014
30. Sinha, P. K., Torres-Bacete, J., Nakamaru-Ogiso, E., Castro-Guerrero, N., Matsuno-Yagi, A., and Yagi, T. (2009) Critical roles of subunit NuoH (ND1) in the assembly of peripheral subunits with the membrane domain of *Escherichia coli* NDH-1. *J. Biol. Chem.* **284,** 9814–9823
31. Torres-Bacete, J., Sinha, P. K., Sato, M., Patki, G., Kao, M. C., Matsuno-Yagi, A., and Yagi, T. (2012) Roles of subunit NuoK (ND4L) in the energy transducing mechanism of *E. coli* NDH-1 (NADH:quinone oxidoreductase). *J. Biol. Chem.* **287,** 42763–42772
32. Galkin, A. S., Grivennikova, V. G., and Vinogradov, A. D. (1999) $\rightarrow H^+/2(e^-)$ stoichiometry in NADH-quinone reductase reactions catalyzed by bovine heart submitochondrial particles. *FEBS Lett.* **451,** 157–161
33. Steimle, S., Bajzath, C., Dörner, K., Schulte, M., Bothe, V., and Friedrich, T. (2011) The role of subunit NuoL for proton translocation by the respiratory complex I. *Biochemistry* **50,** 3386–3393
34. Dröse, S., Krack, S., Sokolova, L., Zwicker, K., Barth, H. D., Morgner, N., Heide, H., Steger, M., Nübel, E., Zickermann, V., Kerscher, S., Brutschy, B., Radermacher, M., and Brandt, U. (2011) Functional dissection of the proton pumping modules of mitochondrial complex I. *PLoS Biol.* **9,** e1001128
35. Amarneh, B., and Vik, S. B. (2003) Mutagenesis of subunit N of the *Escherichia coli* complex I. Identification of the initiation codon and the sensitivity of mutants to decylubiquinone. *Biochemistry* **42,** 4800–4808
36. Euro, L., Belevich, G., Verkhovsky, M. I., Wikström, M., and Verkhovskaya, M. (2008) Conserved lysine residues of the membrane subunit NuoM are involved in energy conversion by the proton-pumping NADH: ubiquinone oxidoreductase (complex I). *Biochim. Biophys. Acta* **1777,** 1166–1172
37. Nakamaru-Ogiso, E., Yano, T., Yagi, T., and Ohnishi, T. (2005) Characterization of the iron-sulfur cluster N7(N1c) in the subunit NuoG of the proton-translocating NADH-quinone oxidoreductase from *Escherichia coli*. *J. Biol. Chem.* **280,** 301–307
38. Takano, S., Yano, T., and Yagi, T. (1996) Structural studies of the proton-translocating NADH-quinone oxidoreductase (NDH-1) of *Paracoccus denitrificans*. Identity, property, and stoichiometry of the peripheral subunits. *Biochemistry* **35,** 9120–9127
39. Castro-Guerrero, N., Sinha, P. K., Torres-Bacete, J., Matsuno-Yagi, A., and Yagi, T. (2010) Pivotal roles of three conserved carboxyl residues of the NuoC (30k) segment in the structural integrity of proton-translocating NADH-quinone oxidoreductase from *Escherichia coli*. *Biochemistry* **49,** 10072–10080
40. Link, A. J., Phillips, D., and Church, G. M. (1997) Methods for generating precise deletions and insertions in the genome of wild-type *Escherichia coli.* Application to open reading frame characterization. *J. Bacteriol.* **179,** 6228–6237
41. Kao, M. C., Di Bernardo, S., Nakamaru-Ogiso, E., Miyoshi, H., Matsuno-Yagi, A., and Yagi, T. (2005) Characterization of the membrane domain subunit NuoJ (ND6) of the NADH-quinone oxidoreductase from *Escherichia coli* by chromosomal DNA manipulation. *Biochemistry* **44,** 3562–3571
42. Laemmli, U. K. (1970) Cleavage of structural proteins during the assembly of the head of bacteriophage T4. *Nature* **227,** 680–685
43. Schägger, H., and von Jagow, G. (1991) Blue native electrophoresis for isolation of membrane protein complexes in enzymatically active form. *Anal. Biochem.* **199,** 223–231
44. Yagi, T. (1986) Purification and characterization of NADH dehydrogenase complex from *Paracoccus denitrificans*. *Arch. Biochem. Biophys.* **250,** 302–311
45. Matsushita, K., Ohnishi, T., and Kaback, H. R. (1987) NADH-ubiquinone oxidoreductases of the *Escherichia coli* aerobic respiratory chain. *Biochemistry* **26,** 7732–7737
46. Yano, T., Sled', V. D., Ohnishi, T., and Yagi, T. (1996) Expression and characterization of the flavoprotein subcomplex composed of 50-kDa (NQO1) and 25-kDa (NQO2) subunits of the proton-translocating NADH-quinone oxidoreductase of *Paracoccus denitrificans*. *J. Biol. Chem.* **271,** 5907–5913
47. Screpanti, E., and Hunte, C. (2007) Discontinuous membrane helices in transport proteins and their correlation with function. *J. Struct. Biol.* **159,** 261–267
48. Ohnishi, T. (2010) Structural biology. Piston drives a proton pump. *Nature* **465,** 428–429
49. Belevich, G., Knuuti, J., Verkhovsky, M. I., Wikström, M., and Verkhovskaya, M. (2011) Probing the mechanistic role of the long α-helix in subunit L of respiratory Complex I from *Escherichia coli* by site-directed mutagenesis. *Mol. Microbiol.* **82,** 1086–1095
50. Yagi, T. (1990) Inhibition by capsaicin of NADH-quinone oxidoreductases is correlated with the presence of energy-coupling site 1 in various organisms. *Arch. Biochem. Biophys.* **281,** 305–311
51. Satoh, T., Miyoshi, H., Sakamoto, K., and Iwamura, H. (1996) Comparison of the inhibitory action of synthetic capsaicin analogues with var-

ious NADH-ubiquinone oxidoreductases. *Biochim. Biophys. Acta* **1273,** 21–30
52. Michel, J., DeLeon-Rangel, J., Zhu, S., Van Ree, K., and Vik, S. B. (2011) Mutagenesis of the L, M, and N subunits of complex I from *Escherichia coli* indicates a common role in function. *PLoS ONE* **6,** e17420
53. Verkhovskaya, M., and Bloch, D. A. (2013) Energy-converting respiratory Complex I. On the way to the molecular mechanism of the proton pump. *Int. J. Biochem. Cell Biol.* **45,** 491–511
54. Larkin, M. A., Blackshields, G., Brown, N. P., Chenna, R., McGettigan, P. A., McWilliam, H., Valentin, F., Wallace, I. M., Wilm, A., Lopez, R., Thompson, J. D., Gibson, T. J., and Higgins, D. G. (2007) Clustal W and Clustal X version 2.0. *Bioinformatics* **23,** 2947–2948